



Journal of Statistical Software

MMMMMM YYYY, Volume VV, Issue II.

<http://www.jstatsoft.org/>

SILIA: Software Implementation of a Lock-in Amplifier for the Extraction of Periodic Features From Data

Amrut Nadgir

University of California Berkeley
and Lawrence Berkeley National
Laboratory

Richard Thurston

University of California Berkeley
and Lawrence Berkeley National
Laboratory

Kirk Larsen

University of California Berkeley
and Lawrence Berkeley National
Laboratory

Niranjan Shivaram

Lawrence Berkeley
National Laboratory

Matthew M. Brister

Lawrence Berkeley
National Laboratory

Daniel S. Slaughter

Lawrence Berkeley
National Laboratory

Abstract

We describe **SILIA**, a software implementation of a multi-channel, multi-frequency Lock-in Amplifier to extract modulated signals from noisy data distributed over collections of channels with arbitrary dimensionality and size. This software implementation emulates the functionality of a multi-channel, multi-frequency lock-in amplifier in a post-processing step following data acquisition. Unlike most traditional lock-in amplifiers, SILIA can work with any number of input channels and is especially useful to analyze data with a high dimensionality. We demonstrate the versatility and performance for extracting weak signals in spectroscopy and fluorescence microscopy. We also discuss more general applications and exhibit a method to automatically estimate error from a lock-in result.

Keywords: lock-in amplifier, multi-channel, spectroscopy, microscopy, time series.

1. Introduction

Lock-in amplifiers are widely used to suppress noise from a periodic signal input with a known frequency. These applications include various types of spectroscopy and other fields including, but not limited to impedance spectroscopy [33], deep level transient spectroscopy [3], and neuroscience [15]. Many multi-channel and multi-frequency lock-in amplifiers are expensive and offer little or no flexibility in the number of input channels and references. By implementing a software lock-in amplifier, we adopt the approach where the amplification is a post-processing step after the data acquisition is completed. A software implementation increases the adaptability of the software to the task at hand and simplifies the lock-in process so it can be easily modified to different specifications.

The present Software Implementation of a Lock-In Amplifier (SILIA) can be used to analyze data from a suitably modulated system, having any number of signal channels and frequency references. As a result, it can serve as a simple yet flexible and cost effective alternative for hardware lock-in amplifiers that are commonly used for multi-channel and multi-frequency applications. Many of the experiments and techniques involving lock-in amplification, such as lock-in imaging [21, 27, 12, 23], pump-probe spectroscopy [6, 20, 16, 13] and pump-probe microscopy [11, 10], require the use of specialty hardware that can perform the necessary computations during the course of the experiment. With SILIA, researchers can use standard recording devices during the experiment and perform lock-in amplification afterwards with no additional cost apart from the requirement to store all the data. SILIA is most applicable to high dimensional data with many channels but is not designed to analyze large datasets which cannot be stored locally.

SILIA offers additional benefits not available to traditional lock-in amplification. One, it can interface with any time series in a specified format. Two, it has the capability to repeatedly retrieve the signal amplitude and relative phase of a weak signal after the initial data acquisition while modifying input parameters and performing post-processing analysis. Lastly, the software is customizable and readily adapted to a wide variety of spectroscopic or imaging instrumentation, and other devices. Since SILIA is applied as a post-processing step, the speed of the data acquisition is only limited by the digital instrumentation and there are no additional hardware optimizations required for execution. The software can also easily be manipulated to suppress noise from varied forms of measurement, such as frequency sweeps [31]. SILIA is also able to estimate the error in the results by partitioning the input signal into overlapping intervals and locking into each of these subintervals.

In this article, we will first discuss the principles behind lock-in amplification and how SILIA implements them in software. After explaining how SILIA works, we move on to a basic multi-signal functionality test for the software where we showcase SILIA’s ability to perform lock-in on multiple channels and references simultaneously and produce an accurate estimation of the error for its result. Then, we benchmark the runtime and noise suppression abilities of SILIA in Section 4. After benchmarking, we apply SILIA to spectroscopy and a fluorescence microscopy simulation and present the results. Finally, we discuss the benefits, drawbacks of SILIA, as well as its potential for improvement. In addition, comprehensive coding examples and tutorials can be found on our Git repository.

1.1. Lock-in Amplification Basics

The lock-in amplifier is able to accomplish noise suppression and phase detection by using

phase-sensitive techniques to remove the fourier components of the input signal that are not modulated at the desired frequency. Lock-in amplifiers generally perform signal mixing and low-pass filtering [19]. The signal mixing step multiplies the input signal by a reference. A sinusoidal reference ensures that the fourier components of the input signal that oscillate at the reference frequency are shifted to 0Hz in the frequency space representation of the mixed signal. A low-pass filter suppresses the frequency components of the mixed signal that are far from 0Hz. After the Lock-in process is completed, the filtered signal output will only contain the fourier components of the input signal that were oscillating at the initial reference frequency, thus suppressing noise. The phase of the signal relative to the reference can be extracted by comparing output between the in-phase and quadrature components of the reference [19, 29, 36].

Early lock-in amplifiers were analog devices, while most modern lock-in amplifiers are fully digital or implemented on a field programmable gate array. Digital lock-in amplifiers tend to be simpler than their analog counterparts, while also achieving wider bandwidth, greater adjustability and improved accuracy [22, 38, 32, 15, 8]. Despite the versatility and broad applications for digital lock-in amplifiers, there are relatively few examples of software implementations of lock-in amplifiers, particularly with highly parallel measurement capabilities for multiple channels and multiple reference frequencies.

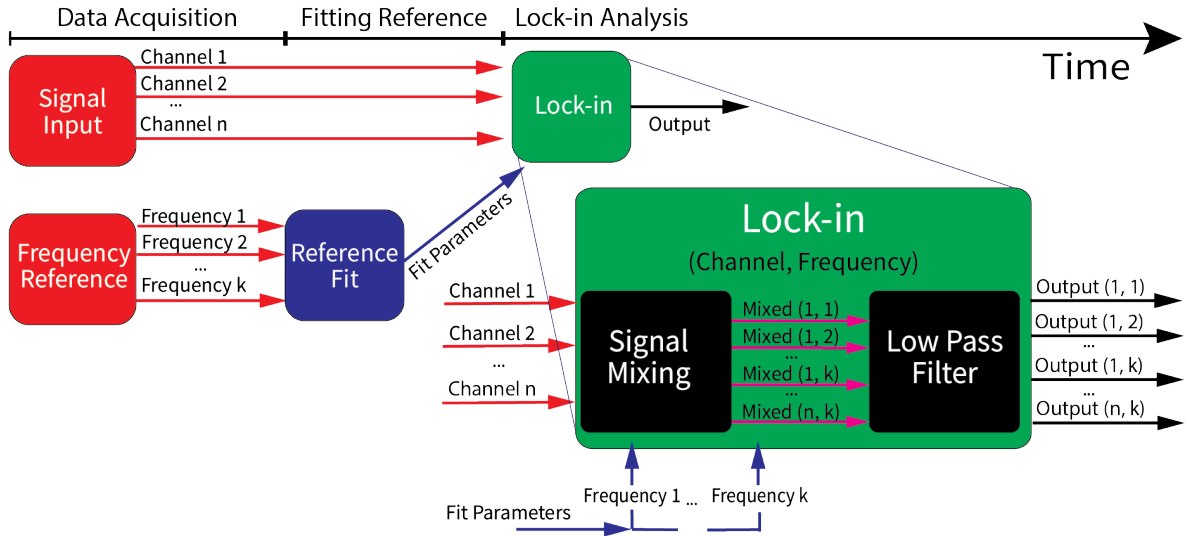


Figure 1: An overview of a single data acquisition cycle and lock-in process, showing the different steps required for the software lock-in analysis in temporal order. The final lock-in amplification step requires the signal data over all n channels and the k fitted frequency references as inputs. The signal mixing and low-pass filter steps are run on the input channels and references where every channel and reference pair is locked into separately. SILIA also has the option to skip the reference fit step.

2. SILIA: Software Implementation of a Lock-In Amplifier

An overview of the software is shown in Figure 1. SILIA fits a sinusoidal function to the references and locks into each input channel with each reference frequency. If there are n

4 **SILIA**: Software Implementation of a Multi-Channel, Multi-Frequency Lock-in Amplifier

input channels and k desired frequency references to lock-in to, then the software will output nk lock-in results.

SILIA requires the raw input signal for each channel, frequency references and a cutoff frequency for the low-pass filter. The raw input and frequency references are not passed into the software in real time and are processed after the data acquisition period. The data acquisition device will be required to store its measurements with timestamps in a format that will later be readable to the software.

For each reference, we compute the in-phase and quadrature mixed components for each signal channel. To mitigate error from nonuniform sampling rates, SILIA has the option to perform linear interpolation on the input signal to ensure evenly spaced samples. Regularly spaced samples are necessary because the Fast-Fourier Transform (FFT) algorithm we use in later parts of the analysis assumes the samples are evenly spaced. The software then applies a low-pass filter to each of the mixed signals. To implement a low-pass filter in software, we applied the real FFT with a Hanning window to the mixed signal and removed all components outside a symmetric interval centered on 0, with the width specified by a frequency cutoff parameter. This acts as a low-pass filter with a response curve that is essentially a step function, thus minimizing any error caused by the filtering step in conventional lock-in amplifiers, but also assumes that samples are evenly spaced (uniform sampling). Due to the discrete sampling of the signal input, the filter cannot differentiate between arbitrarily close frequency components of the signal. Therefore, the cutoff frequency is limited by the frequency resolution of the measured signal. Assuming nearly uniform sampling, the frequency resolution tends to improve with more data. In addition, the maximum frequency that can be locked into is given by $f/2$ and is equal to the Nyquist frequency of the data. Lock-in amplitudes and phases were computed from the measured in-phase and quadrature components of the filtered signals [5]. Each data acquisition cycle produces an array of output values indexed by their respective channel and frequency reference (Fig. 1).

The fitted references are scaled so the output when locking into a purely sinusoidal signal that oscillates at the reference frequency is equal to the amplitude of the input. There can be additional, but predictable bias when the input waveform is non-sinusoidal. The most common example of this is with square wave inputs. The fourier series expansion of an even square wave with a peak to peak amplitude of A and a duty cycle d is $\frac{2A}{\pi} \sum_{n=1}^{\infty} 1/n \sin(n\pi d) \sin(2n\pi ft)$ where t is time and f is the frequency of the square wave in Hz. As long as the cutoff frequency of the lock-in is less than f , only the $n = 1$ fourier component will remain after the low-pass filter. Therefore, the ideal lock-in output magnitude for a standard square wave signal with a duty cycle of $1/2$ would be $2A/\pi$. Since this type of bias is predictable, it can also easily be accounted for.

SILIA also has the ability to estimate inner products in frequency space between the reference and the input signal. To compute these projections, SILIA has the option to skip the reference fitting step and mix the signal input with a scaled raw reference. The raw reference is scaled by a factor of 2 so the inner product between two purely sinusoidal signals that oscillate at the same frequency is the product of their amplitudes. This feature gives SILIA the ability to perform lock-in on non-sinusoidal references, but it cannot extract phase information in this case due to a lack of knowledge about the structure of the reference input.

SILIA has an additional built-in error estimation feature. Apart from the primary lock-in functionality, it can split the input signal into portions that may or may not overlap

and lock into each part. After splitting and locking into the data, SILIA evaluates the standard deviation of the results. The size and number of these portions are specified by input parameters. There is a tradeoff to be made here since too little overlap and too many windows will result in an overestimation of the error, while too few windows with very large window sizes and high overlap will underestimate the error.

3. Error Estimation Analysis

3.1. Methods

We performed a series of simulations to test the lock-in capabilities of SILIA for multiple channels and multiple references acquired simultaneously, and to characterize the quality of the output lock-in signal and phase compared to the input signals and references. Specifically, we wanted to test the error estimation functionality of SILIA.

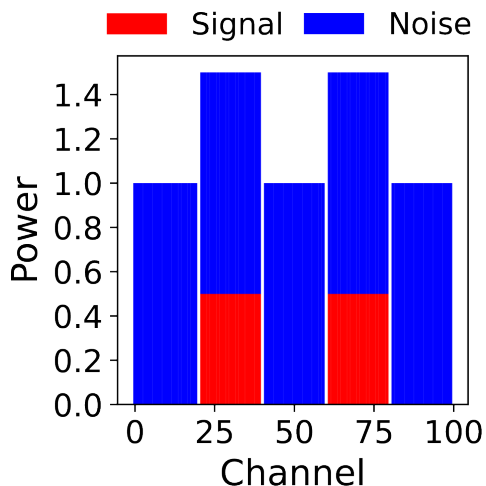


Figure 2: A graphical representation of the SNR for each channel of the input signal. We simulated 100 channels, which we split into batches of 20 channels each. The first, third and fifth batch of 20 channels were Gaussian noise with a variance, or power of one. The second and fourth batches were sine waves with a power of $1/2$ and additional Gaussian Noise. One of the sine waves oscillated at 80Hz (channels 20-40) while the other had a frequency of 120Hz (channels 60-80).

For the data acquisition component of the simulation, we simulated 100 channels of data, some of which had only Gaussian noise while others had a synthetic signal, modulated at a specific reference frequency, as well as the noise. The signal was sinusoidal and had a power of $1/2$ while the noise had a variance of 1 (Fig. 2). We adopt the convention of SNR defined as $\frac{\text{signal power}}{\text{noise power}}$. Therefore, the SNR in this simulation was $1 : 2$ for the channels that contained the input signals and the signal had an amplitude of 1.

The data acquisition is for a simulated time of 5 seconds at a sampling rate of 5000Hz and a frequency resolution of 0.2Hz. The cutoff frequency is also set to 0.2Hz. The references are 80Hz and 120Hz square waves.

6 **SILIA**: Software Implementation of a Multi-Channel, Multi-Frequency Lock-in Amplifier

Output values are generated by using SILIA to lock into 80Hz and 120Hz references. Uncertainties are estimated by separately analyzing four evenly spaced time-intervals, each of which contains a third of the input data, and computing the standard deviation of the output lock-in magnitude and phase across all intervals. The noise power is twice as large as the signal power (Fig. 2).

3.2. Results

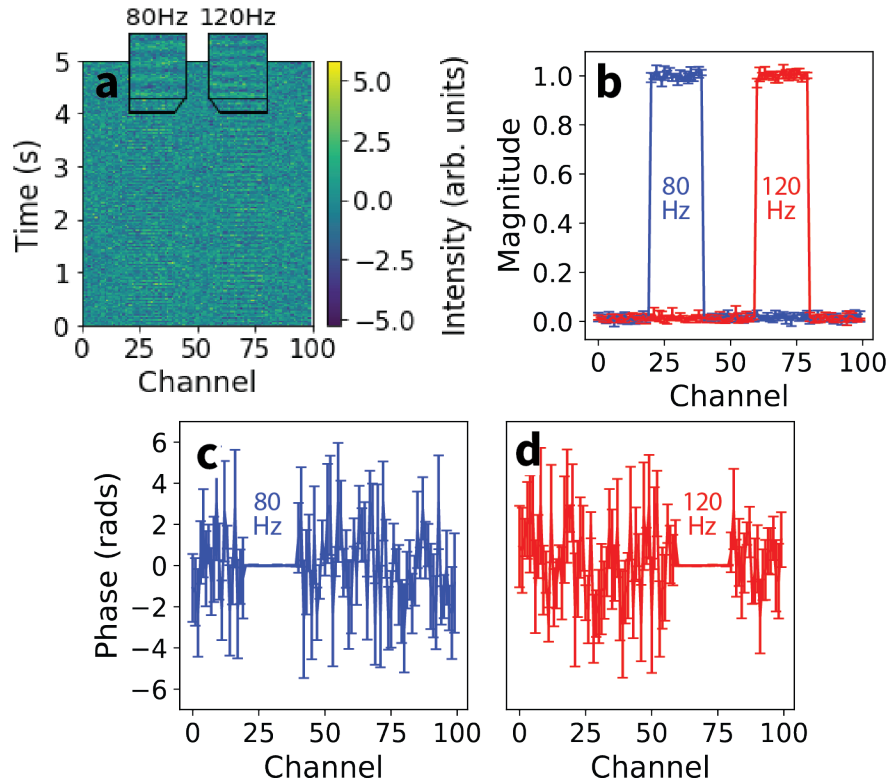


Figure 3: (A) Spectrogram of the simulated signal. The two zoomed insets show the noisy oscillating signals in channels 20-40 and 60-80, both signals oscillate at different frequencies. (B) The multi-frequency SILIA outputs. Both curves correctly identify the amplitudes of the 80Hz and 120Hz signals at each channel. The output for each channel at the peaks are equal, within the estimated uncertainties, and the uncertainties are greater when there is no signal present. (C, D) Phase output when locking into both frequencies. We see that the phase error is very small in the presence of signal and large for all noisy channels.

Freq.	Magnitude Error		Phase Error	
	Predicted	Actual	Predicted	Actual
80Hz	0.016	0.008	0.011	0.006
120Hz	0.017	0.012	0.011	0.008

Table 1: A comparison of the errors predicted by the error estimation feature of SILIA with the actual standard deviation of SILIA output over relevant channels.

The input consisted of two sinusoidal signals oscillating at 80Hz and 120Hz respectively with an amplitude of 1 and higher-amplitude additional Gaussian noise distributed over each channel (Fig. 3A). We expect SILIA to suppress the Gaussian noise, as well as any signal not oscillating at the reference frequency. When locking into the 80Hz or 120Hz signal, we should see an output magnitude near 1 for channels 20-40 or 60-80 respectively, and near 0 everywhere else. When locking into the 80Hz and 120Hz signals, we see mean peak values of 1.000 with standard deviations of 0.008 and 0.012 as well as mean outputs in channels without signal of 0.021 and 0.017 respectively which is almost exactly what we expect (Fig. 3B). The error bars at the peak values for the 80 and 120Hz results are, on average, 0.016 and 0.017 which are overestimations of the standard deviation of the output at peak signal by slightly less than a factor of two but still give a useful estimate of fluctuation in output (Fig. 3B, Table 1).

For the 80Hz and 120Hz outputs in the channels having signal, we observe a phase of 0.004 and -0.001 respectively with standard deviations of 0.006 and 0.008 and mean predicted errors of 0.011 (Fig. 3C, D, Table 1). The phase of the results closely match an expected phase of 0 in the presence of signal and the error bars provide a reasonable estimate of the standard deviation in phase results. We also observe fluctuations in phase where signal is not present since SILIA can only extract noise in those channels (Fig. 3C, D).

4. Software Benchmarking

4.1. Methods

To test the speed and effectiveness of the software, we ran a few different benchmarks. Our benchmarking software measured the amount of time it took for SILIA to process different amounts of input data, and also tested the change in the signal to noise ratio (SNR) for different amounts of data.

For our initial benchmarks, we measured the amount of time it took for the software to run for a variable number of input samples, channels and references by varying each of those three parameters individually while holding the other two constant. We used constant values of 4096 samples, 1 channel and 1 reference. This benchmarking allowed us to confirm the linear runtime of SILIA with respect to the data acquisition time, size of each sample and number of signals (Fig. 4).

We also ran benchmarks that quantified the percentage error of the output magnitude while varying the number of simulated input signal cycles and the samples per cycle with constant parameters of 10 samples per cycle and 5000 cycles respectively. We added Gaussian noise to the input with varying standard deviations and the input signal was a sinusoidal wave with an amplitude of 1. Our results were averaged over 100 runs and compared with a theoretical estimate of the results from signal averaging given by σ^2/n where σ^2 is the variance of the noise and n is the number of cycles (Fig. 5A-D).

We additionally quantified the reaction of our lock-in to a class of non-sinusoidal waveforms. Due to their commonality, we chose to use 100Hz square waves with peak to peak height of 1 and varying duty cycles. After generating the signals and running the lock-in, we proceeded to confirm that our results matched the primary Fourier component of the signal (Fig. 5E).

To visualize the response curve of the low-pass filter, we varied the simulated signal frequency to $100 \pm 5\text{Hz}$ but kept the reference frequency constant at 100Hz. The input signal was a

8 **SILIA**: Software Implementation of a Multi-Channel, Multi-Frequency Lock-in Amplifier

sinusoidal wave with an amplitude of 1 and had no additional noise added to it. We plotted the lock-in output magnitude with respect to the input signal frequency with effective cutoffs of 0.06Hz and 1.02Hz (Fig. 5F).

4.2. Results

The results from benchmarking help quantify the time complexity of SILIA, as well as its reaction to different sources of error. By quantifying the different aspects of this software implementation, we are able to better highlight its strengths and limitations.

Runtime Benchmarking

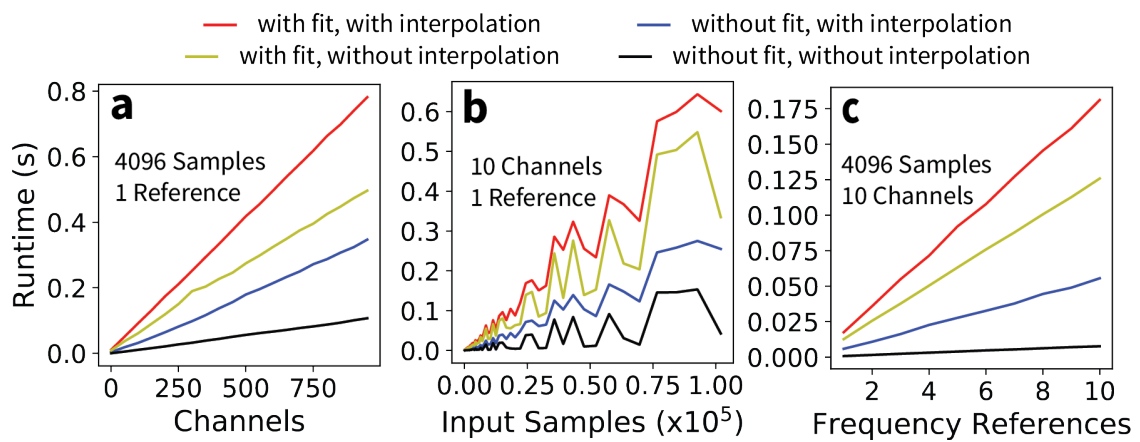


Figure 4: Dependence of the runtime of SILIA on the number of channels, input samples, and frequency references. (A, C) There is a linear dependence of runtime on the number of input channels and frequency references. (B) Shows a general linear relationship between the runtime and data acquisition time, but there is nonlinearity introduced by the slower runtime of the Fourier Transform when the number of input samples is not a power of 2.

As the number of input channels increases, the total runtime of the software rises proportionally (Fig. 4A). We see a similar trend with the number of frequency references, where adding an additional reference frequency to the SILIA input will increase the runtime of the software by a constant amount (Fig. 4C). Both trends can be attributed to the software essentially performing the analysis separately and in sequential order for each channel and frequency reference. We also observe a general linear increase in runtime with respect to the number of input samples but see nonlinear fluctuations which result in increased runtimes when the number of input samples is not close to a power of 2 (Fig. 4B). This is likely due to our use of the radix-2 FFT algorithm, which has a runtime that is optimized for input sample sizes that are a power of 2 [24, 2]. As expected, we see that SILIA is slowest when asked to fit the reference signal and interpolate the input, and is significantly faster when the user skips those steps. In addition, it is apparent that using a fitted reference is more costly than applying interpolation to the input signal (Fig. 4). This is due to the additional requirement of computing phase when the reference is fitted.

It is important to note that these benchmark plots do not necessarily reflect the exact runtime of the software in general, since those runtimes are dependent on the hardware used to run

SILIA and potential new optimizations in the code. The observed linear trends imply that the post-processing time will generally be proportional to the data acquisition time.

Error Benchmarking

When benchmarking the effects of experimental errors, we focused on three potential sources of uncertainties - Gaussian or oscillating noise in the input signal, low-pass filter response and non-sinusoidal signal. A low-pass filter response with low roll-off can introduce unwanted artifacts from frequencies outside the cutoff range into the result of the lock-in amplification, and, as mentioned in Section 2, non-sinusoidal input can introduce bias into the result.

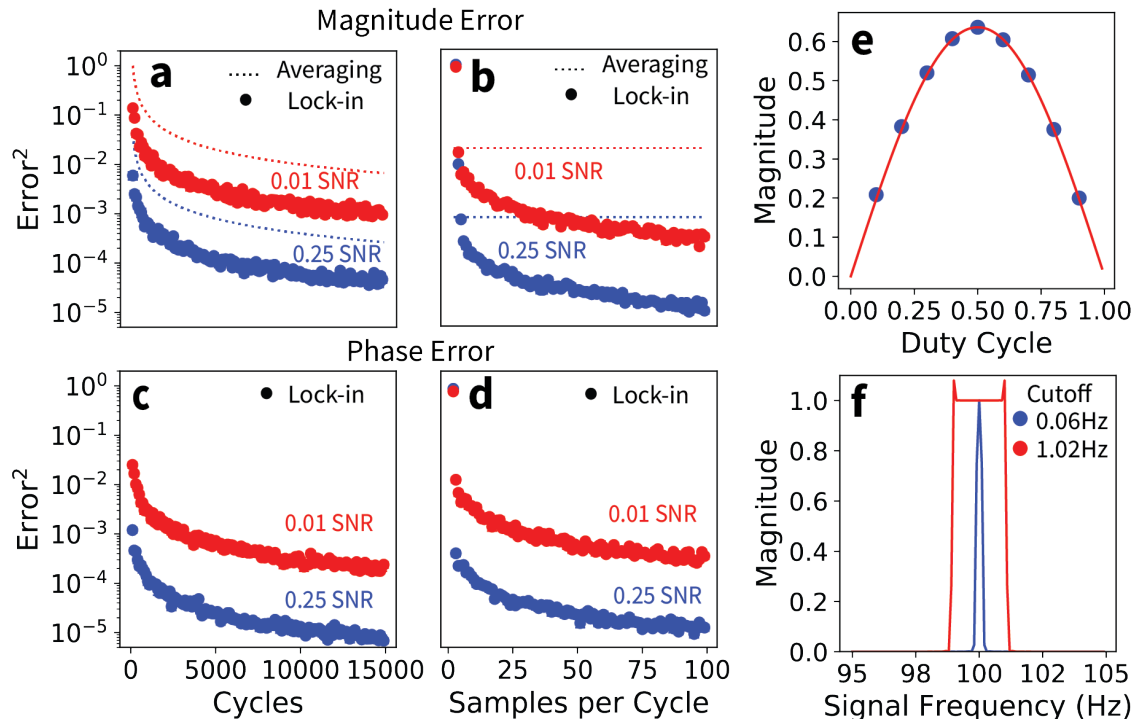


Figure 5: (A, B) Dependence of Mean Square Error on output magnitude with respect to input sampling. There is a steep decrease in error with respect to total data acquisition time (Fig. A) and sampling rate (Fig. B). By comparison, we see that SILIA produces superior results to averaging each cycle of data. (C, D) SILIA phase output rapidly increases in accuracy with respect to the number of input cycles (Fig. C) and the sampling rate (Fig. D). (E) Output as a function of the duty cycle of a square wave input signal. SILIA outputs are fit to the red curve, which is the first term in the Fourier series expansion of a square wave with varied duty cycles. We calculated $r^2 = 1.0$ using the residuals of a fit to the curve $2\pi \sin(\pi d)$, where d is the duty cycle. (F) Low-pass response curve for a constant reference frequency of 100Hz.

Output error of lock-in amplifiers tends to decrease sharply with respect to data acquisition time and SNR [5, 22, 37, 26]. We see a similar significant improvement in the output error with respect to increased data acquisition time (Fig. 5A, C), and can conclude the necessity of longer data acquisition times for more accurate results, especially from data with low SNR. We see that larger sampling rates yield reduced output error (Fig. 5B, D) and that SILIA outperforms signal averaging (Fig. 5A, B). The squared error from signal averaging

was calculated using the theoretical standard of Variance = $\frac{\text{Noise Power}}{\text{Number of Cycles}}$. The shape of the input signal waveform affects the output in an easily quantifiable manner. We observe that the output when locking into square waves with different duty cycles closely matches the primary Fourier component of the input signal, as expected (Fig. 5E). Furthermore, the significant decrease in the output magnitude when the input oscillates outside the cutoff frequency range (Fig. 5F) demonstrates the effectiveness of SILIA at filtering out periodic noise.

5. Applications of SILIA

5.1. Spectral Analysis

Methods

To test SILIA in an experimental setting, we used the Ocean Optics OCEAN-FX-XR1-ES spectrometer to measure amplitude-modulated laser light, and the fluorescence spectrum emitted from a dye that was excited by 532 nm laser pulses from a ThorLabs CPS532 diode-pumped solid state laser with a continuous-wave power of 4.5mW (Fig. 6). To modulate the amplitude of the signal and measure a frequency reference, we used a National Instruments USB6001 data acquisition device connected to a Thorlabs MC2000B chopper.

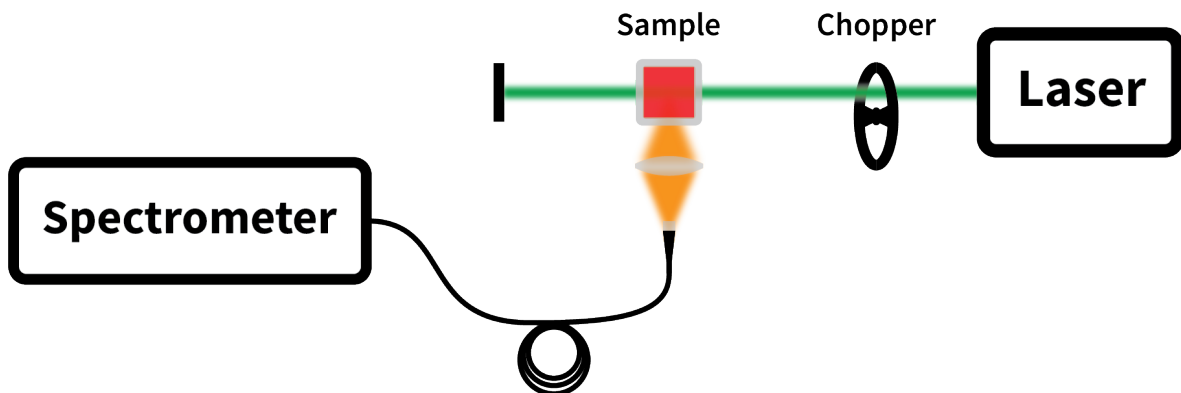


Figure 6: Experimental setup to measure the fluorescence spectrum of a Rhodamine 6G sample and test whether SILIA can suppress noise from our measurement. A chopper wheel is used to modulate the laser which excites the Rhodamine while a lens is used to focus the resulting fluorescence signal into the spectrometer.

During the data acquisition, we used spectrometer readings from a wavelength range from 490nm to 700nm and a wavelength resolution with a mean of 0.42nm and standard deviation of 0.02nm ($0.42 \pm 0.02\text{nm}$). We measured our reference input with a 2000Hz sampling rate from the chopper and chopped the laser at 100Hz for the laser spectrum measurement. The sampling rate of the spectrometer was $230 \pm 49\text{Hz}$, with a two second runtime per data acquisition cycle for three cycles. Using SILIA, we locked into the spectrometer signal in an attempt to suppress any background noise in our measurement (Fig. 7).

For the fluorescence spectrum measurement, we induced fluorescence in 1.3mM, 0.13mM and 0.013mM 95% purity Rhodamine 6G samples in ethanol and measured the output spectrum with the same wavelength range and resolution as mentioned above (Fig. 6). We used a 250.0 mm convex lens to focus the fluorescence signal into the spectrometer. The laser was chopped at 50Hz and our reference input was measured from the chopper with a 2000Hz sampling rate. For this measurement the sampling rate of the spectrometer was $249 \pm 58\text{Hz}$, with a three second runtime per data acquisition cycle for three cycles. We used SILIA to lock into the fluorescence signal and compared our results to the PhotoChem database (Fig. 8) [35, 34].

During the analysis, we fitted the reference signal but did not use interpolation. We also subtracted signal offset prior to using SILIA on the data.

Results

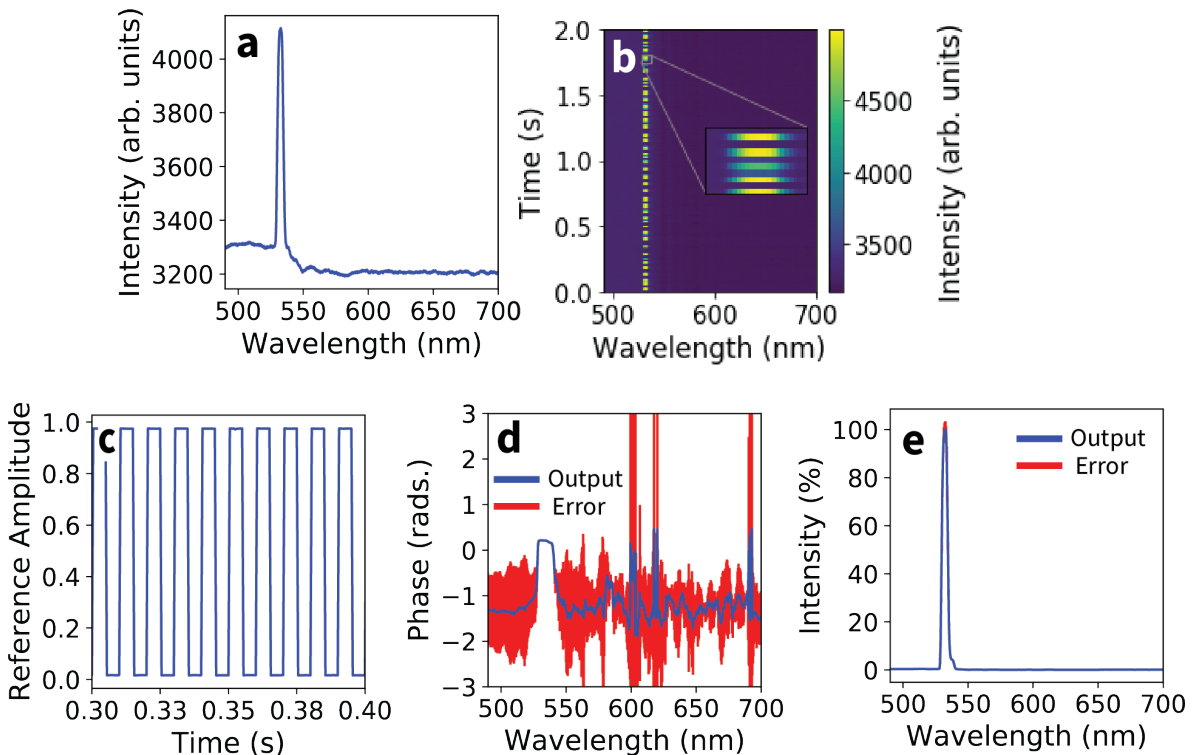


Figure 7: (A) The time-averaged signal of the spectrometer. The peak from the chopped laser signal can be seen at 532nm. (B) A spectrogram of the chopped laser signal from a single data acquisition cycle of the spectrometer, showing the 100Hz oscillation of the signal input. Irregular sampling of light by the spectrometer leads to intensity variations of $\pm 33\%$ in laser peaks. (C) The optical chopper output signal and frequency reference over time, which shows 100 ± 1 Hz oscillation. (D) SILIA output phase averaged over three data acquisition cycles demonstrating phase convergence in the presence of signal. (E) SILIA output magnitude averaged over three data acquisition cycles showcasing a clear laser signal.

SILIA output suppresses background signal (Fig. 7A) and cleanly illustrates the peak of the laser signal at 532nm (Fig. 7E) and suppresses background signal (Fig. 7A). Over the three

data acquisition cycles, the peak value of the output fluctuated with a standard deviation of 5.7% (Fig. 7E) which is likely due to the inconsistencies in the spectrometer measurement (Fig. 7B). We see the expected fluctuations in phase in the presence of no signal, as well as a clear convergence in phase near 532nm (Fig. 7D). The phase convergence between wavelengths demonstrates the expected correlation in the output between wavelengths with signal, whereas lack of error in the phase convergence region indicates the experimental setup was consistent over the three data acquisition cycles.

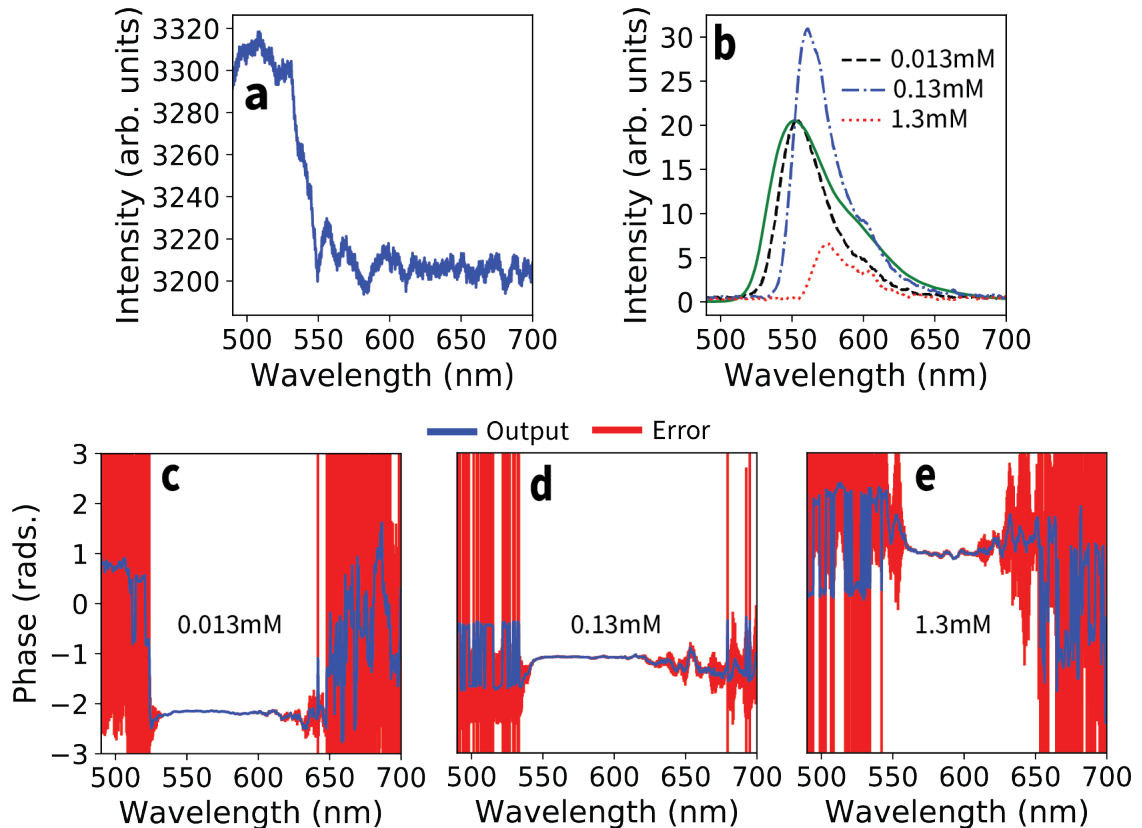


Figure 8: (A) Typical time-averaged signal of the spectrometer. The rhodamine spectrum is invisible in the spectrometer readings. (B) SILIA output for different concentrations of Rhodamine averaged over 3-5 data acquisition cycles. The peaks become more distorted with increasing Rhodamine concentration and have varying heights due to the primary and secondary inner-filter effects. The spectra are plotted against the green curve, a rescaled reference rhodamine 6G fluorescence measurement [35, 34]. Our 0.013mM results closely match the reference despite being taken with inferior equipment. Output peaks shift to higher wavelengths when rhodamine concentration is increased. (C,D,E)) SILIA phase output for the various concentrations of rhodamine. We observe a consistent phase convergence across all three concentrations in the presence of signal.

As another demonstration of the robustness of the SILIA approach, we used its capabilities to perform lock-in on a rhodamine fluorescence signal without using a photomultiplier following optical excitation at 532 nm, where the output magnitude illustrates a rhodamine spectrum peak (Fig. 8B) that was initially invisible in the presence of background noise (Fig. 8A). The

SILIA output closely matches a rhodamine 6G fluorescence spectrum from the PhotoChem database [35, 34], shown as the green curve, and we observe that higher concentrations of rhodamine result in fluorescence peaks at higher wavelengths with increased distortions (Fig. 8B). We can attribute these distortions to a primary inner filter effect which was observed during data acquisition. In addition, we observe a discrepancy in the heights of the peaks (Fig. 8B). The 0.013mM peak was lower than the 0.13mM peak due to an observed secondary inner filter effect and the 1.3mM peak was the smallest due to significant observed primary inner filter effect. As expected, we also see a consistent phase convergence in the presence of signal and note that the convergence is stronger at lower Rhodamine concentrations (Fig. 8C,D,E). This is consistent with our previous observation that the spectra from lower Rhodamine concentrations better agreed to the reference spectrum.

5.2. Imaging Simulation

Methods

SILIA is designed to work with signal inputs of arbitrary dimensionality. To demonstrate the potential application to analyze microscopy data, we used an experimental fluorescence microscopy image of liver cells (Fig. 9A, B, C) [18]. Lock-in amplification can be used on microscopy data to extract a fluorescence signal from noise [23] and we demonstrate the use of SILIA for such experiments.

To simulate a fluorescence signal, we multiplied the image by a square wave with a peak to peak height of 1 so it would periodically flash on and off. We took 500 total samples of this square wave at 10 samples per cycle. The microscope image was in a RGB format and had a size of 450x508 pixels which resulted in an input signal of 685800 channels. Each RGB value in the image can range from 0 to 255, where the values of (0, 0, 0) represents a black color and (255, 255, 255) represents a white color. We added a significant amount of Gaussian noise with a standard deviation of 75 to each pixel and ran the lock-in amplification on the image signal.

To demonstrate the applicability of this technique on an image with a higher brightness, we repeated the simulation using an image of a lightsaber. This image had a size of 298x444 pixels and was an RGB image, which resulted in an input signal of 396936 channels. We added the same Gaussian noise and used SILIA to recover the original image (Fig. 9D,E,F).

Results

We seek to recover the original microscopy image of the clean signal (Fig. 9A) from the noisy signal (Fig. 9B) by using SILIA. We observe that the cells are barely visible in the noisy signal (Fig. 9B). Using SILIA, we were able to accurately recover the colors, locations and shapes of the cells but with diminished output (Fig. 9C-Left). Since the input signals are square waves with a 50% duty cycle, we expect a SILIA output of $2/\pi$ times the original image (Fig. 5D) which results in a dimmer initial output (Fig. 9C-Left). To correct this error, we scale each RGB value by $\pi/2$ and cap the result so no value is above 255 (Fig. 9C-Right). We recover the live cell image (Fig. 9A-Right). We use a similar process for the lightsaber image, where we flash it at the reference frequency (Fig. 9D) and add significant noise (Fig. 9E). With just 500 samples of the signal at 10 samples/cycle, SILIA is able to recover the shape and contours of the lightsaber (Fig. 9F-Left) and by once again scaling the results up by $\pi/2$, we

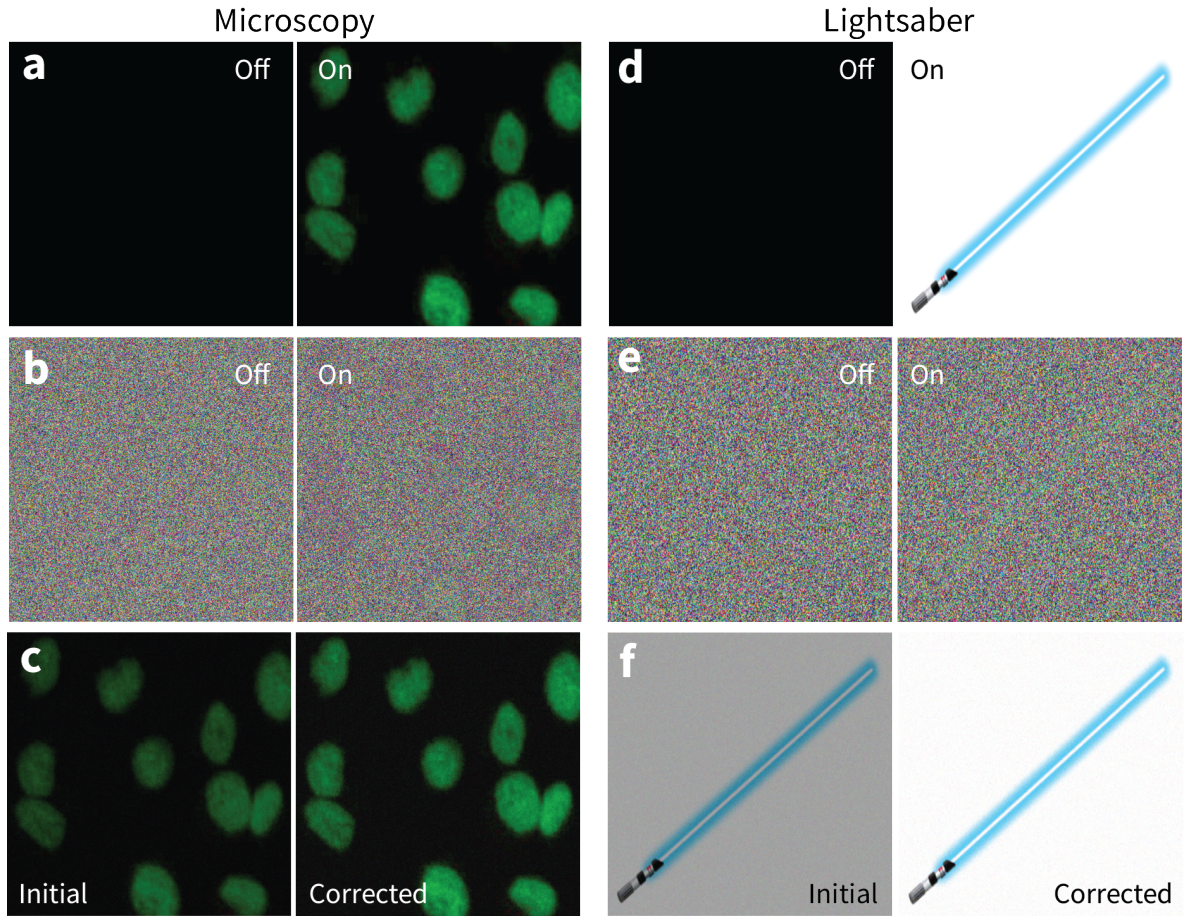


Figure 9: All panels have been scaled to a square aspect ratio. The left half is related to microscopy while the right made use of a lightsaber photo with a white background. (A) Simulated clean fluorescence signal of the sample using a live cell image [18]. The left panel shows the sample when it is not fluorescing and the right panel shows the maximum fluorescence signal. (B) Fluorescence signal with added noise. (C) SILIA recovered the original fluorescence image despite significant noise. The output for the corrected panel is multiplied by $\pi/2$ to compensate for diminished output when locking into a square wave signal. (D,E,F) We repeat the simulation in A, B, C but with an image of a lightsaber with a white background to show the broad applicability of this technique on images with varied color and brightness. The lightsaber is a metaphor for how SILIA “cuts” through noise.

see an accurate representation of the original lightsaber image. SILIA took about 3 minutes to compute this output on a laptop computer with a 2.7 GHz Intel i7 CPU and 16.0 GB RAM.

6. Discussion

SILIA is an inexpensive and general alternative to multi-channel and multi-frequency lock-in amplifiers. Some advantages in the present implementation include convenient capabilities

to estimate error in lock-in results, simplicity compared to other digital lock-in amplifiers, and the flexibility to extract periodic signals having arbitrary dimensionality. For example, the code is readily adaptable to a frequency sweep measurement [31] by fitting the reference to a frequency modulated waveform. Our software provides additional flexibility by working under a paradigm where the lock-in procedure is realized as a post-processing step. As a result, measured data can be reduced or preprocessed prior to performing the lock-in operation, and SILIA can be run multiple times on the same dataset or subsets of a dataset with adjusted input parameters, which is automatically done when computing errors. For example, by artificially scaling the time axis of the reference prior to lock-in, harmonics of the reference frequency can also be applied to recreate a Fourier series approximation to the exact signal waveform in each channel.

Some limitations of using this implementation include the potentially significant runtime of the software when analyzing large datasets. However, there are methods that can significantly shorten the duration of the lock-in process that will be implemented in the future. The software currently has a linear runtime with respect to the number of channels and frequency references (Fig. 4A, C), which can be drastically reduced through parallelization of SILIA with respect to each channel and frequency reference [30, 28, 4]. In the present work, we chose not to pursue parallelization in SILIA after initial attempts of parallelization in Python did not significantly improve runtime for the present datasets. Given a prior knowledge of the number of samples being analyzed, faster FFT algorithms [4, 14, 24, 2, 25, 9] can be chosen. There are also superior techniques to the optional interpolation procedures in the present work, which can be implemented to mitigate error from the FFT due to inconsistent sampling rates [4, 17, 39, 7]. SILIA is also limited in the size of the dataset it can process since it stores all the data in RAM to perform operations on it. However, this can be circumvented in future applications by adding methods to read and write to data storage formats such as csv or even SQL.

We have demonstrated and discussed SILIA’s applications in spectroscopy, microscopy and imaging technologies. SILIA could also be employed to extract periodic features from video data without a separate reference input by using a reference pixel [1].

7. Conclusions

With our software implementation, we have demonstrated a device that can suppress background noise from periodic features in datasets with an arbitrary number of channels and frequency references. By adopting a paradigm where the lock-in amplification is implemented as a post-processing step, we find a higher degree of flexibility than available in other methods while ensuring the lock-in does not hinder or complicate data acquisition. Our implementation is relatively straightforward to edit and we encourage users to improve and customize the code to suit their needs.

8. Acknowledgements

This material is based upon work performed at the Lawrence Berkeley National Laboratory and was supported by the U.S. Department of Energy, Office of Science, Division of Chemical Sciences of the Office of Basic Energy Sciences under Contract DE-AC02-05CH11231.

References

- [1] Davide Alinovi. “Video Processing for Remote Respiration Monitoring”. In: (2018). DOI: [10.5565/rev/elcvia.1124](https://doi.org/10.5565/rev/elcvia.1124).
- [2] Rassoul Amirkattahi. “Calculation of computational complexity for radix-2 p fast fourier transform algorithms for medical signals”. en. In: *Journal of Medical Signals & Sensors* 3.4 (Oct. 2013). Publisher: Medknow Publications, p. 217. ISSN: 2228-7477. DOI: [10.4103/2228-7477.128310](https://doi.org/10.4103/2228-7477.128310). URL: <http://www.jmssjournal.net/article.asp?issn=2228-7477;year=2013;volume=3;issue=4;spage=217;epage=224;aulast=Amirkattahi;type=0> (visited on 07/27/2020).
- [3] F. D. Auret. “Considerations for capacitance DLTS measurements using a lock-in amplifier”. In: *Review of Scientific Instruments* 57.8 (Aug. 1986). Publisher: American Institute of Physics, pp. 1597–1603. ISSN: 0034-6748. DOI: [10.1063/1.1138537](https://doi.org/10.1063/1.1138537). URL: <https://aip.scitation.org/doi/10.1063/1.1138537> (visited on 07/27/2020).
- [4] Alexander H. Barnett, Jeremy Magland, and Ludvig af Klinteberg. “A Parallel Nonuniform Fast Fourier Transform Library Based on an “Exponential of Semicircle” Kernel”. en. In: *SIAM Journal on Scientific Computing* 41.5 (Jan. 2019), pp. C479–C504. ISSN: 1064-8275, 1095-7197. DOI: [10.1137/18M120885X](https://doi.org/10.1137/18M120885X). URL: <https://epubs.siam.org/doi/10.1137/18M120885X> (visited on 08/06/2020).
- [5] Sabyasachi Bhattacharyya et al. “Implementation of Digital Lock-in Amplifier”. en. In: *Journal of Physics: Conference Series* 759 (Oct. 2016). Publisher: IOP Publishing, p. 012096. ISSN: 1742-6596. DOI: [10.1088/1742-6596/759/1/012096](https://doi.org/10.1088/1742-6596/759/1/012096). URL: <https://doi.org/10.1088/1742-6596/759/1/012096> (visited on 07/27/2020).
- [6] S. Bourquin et al. “High-speed femtosecond pump probe spectroscopy with a smart pixel detector array”. en. In: *Optics Letters* 28.17 (Sept. 2003), p. 1588. ISSN: 0146-9592, 1539-4794. DOI: [10.1364/OL.28.001588](https://doi.org/10.1364/OL.28.001588). URL: <https://www.osapublishing.org/abstract.cfm?URI=ol-28-17-1588> (visited on 07/27/2020).
- [7] Emmanuel Candès, Laurent Demanet, and Lexing Ying. “A Fast Butterfly Algorithm for the Computation of Fourier Integral Operators”. In: *Multiscale Modeling and Simulation* 7.4 (June 2009). Number: 4 Publisher: Society for Industrial and Applied Mathematics, pp. 1727–1750. ISSN: 1540-3459. URL: <https://resolver.caltech.edu/CaltechAUTHORS:20091026-135743447> (visited on 08/03/2020).
- [8] M. Carminati et al. “Note: Differential configurations for the mitigation of slow fluctuations limiting the resolution of digital lock-in amplifiers”. In: *Review of Scientific Instruments* 87.2 (Feb. 2016). Publisher: American Institute of Physics, p. 026102. ISSN: 0034-6748. DOI: [10.1063/1.4941721](https://doi.org/10.1063/1.4941721). URL: <https://aip.scitation.org/doi/10.1063/1.4941721> (visited on 07/27/2020).
- [9] Michael Cerna and Audrey F Harvey. “The Fundamentals of FFT-Based Signal Analysis and Measurement”. en. In: (July 2000), p. 20.
- [10] P.-T Dong and J.-X Cheng. “Pump-probe microscopy: Theory, instrumentation, and applications”. In: *Spectroscopy (Santa Monica)* 32 (Apr. 2017), pp. 24–36.

- [11] Martin C. Fischer et al. “Invited Review Article: Pump-probe microscopy”. In: *Review of Scientific Instruments* 87.3 (Mar. 2016). Publisher: American Institute of Physics, p. 031101. ISSN: 0034-6748. DOI: [10.1063/1.4943211](https://doi.org/10.1063/1.4943211). URL: <https://aip.scitation.org/doi/10.1063/1.4943211> (visited on 07/27/2020).
- [12] Sergi Foix, Guillem Alenyà, and Carme Torras. “Lock-in Time-of-Flight (ToF) Cameras: A Survey”. In: *IEEE Sensors Journal* 11.9 (Sept. 2011). Conference Name: IEEE Sensors Journal, pp. 1917–1926. ISSN: 1558-1748. DOI: [10.1109/JSEN.2010.2101060](https://doi.org/10.1109/JSEN.2010.2101060).
- [13] Mizuho Fushitani. “Applications of pump-probe spectroscopy”. en. In: *Annual Reports Section 'C' (Physical Chemistry)* 104.0 (June 2008). Publisher: The Royal Society of Chemistry, pp. 272–297. ISSN: 1460-4787. DOI: [10.1039/B703983M](https://doi.org/10.1039/B703983M). URL: <https://pubs.rsc.org/en/content/articlelanding/2008/pc/b703983m> (visited on 07/27/2020).
- [14] Aravind Ganapathiraju et al. “A Comparative Analysis Of FFT Algorithms”. In: (Feb. 1999).
- [15] Giuseppe Costantino Giaconia et al. “Exploring FPGA-Based Lock-In Techniques for Brain Monitoring Applications”. en. In: *Electronics* 6.1 (Mar. 2017). Number: 1 Publisher: Multidisciplinary Digital Publishing Institute, p. 18. DOI: [10.3390/electronics6010018](https://doi.org/10.3390/electronics6010018). URL: <https://www.mdpi.com/2079-9292/6/1/18> (visited on 07/27/2020).
- [16] Leonid Gilburd et al. “Near-Field Infrared Pump–Probe Imaging of Surface Phonon Coupling in Boron Nitride Nanotubes”. en. In: *The Journal of Physical Chemistry Letters* 7.2 (Jan. 2016), pp. 289–294. ISSN: 1948-7185. DOI: [10.1021/acs.jpclett.5b02438](https://doi.org/10.1021/acs.jpclett.5b02438). URL: <https://pubs.acs.org/doi/10.1021/acs.jpclett.5b02438> (visited on 07/27/2020).
- [17] Leslie Greengard and June-Yub Lee. “Accelerating the Nonuniform Fast Fourier Transform”. en. In: *SIAM Review* 46.3 (Jan. 2004), pp. 443–454. ISSN: 0036-1445, 1095-7200. DOI: [10.1137/S003614450343200X](https://doi.org/10.1137/S003614450343200X). URL: <http://epubs.siam.org/doi/10.1137/S003614450343200X> (visited on 08/03/2020).
- [18] Fatimah Hashim, Faizatul Mehamod, and Naizatul Nawi. “In Vitro Toxicity Evaluation of Caffeine Imprinted Polymer (CAF-MIP) for Decaffeination Method on Normal Chang Liver Cells”. In: *Makara Journal of Technology* 21.1 (Apr. 2017). ISSN: 2356-4539. DOI: [10.7454/mst.v21i1.3075](https://doi.org/10.7454/mst.v21i1.3075). URL: <https://scholarhub.ui.ac.id/mjt/vol21/iss1/4>.
- [19] K. Kishore and S. A. Akbar. “Evolution of Lock-In Amplifier as Portable Sensor Interface Platform: A Review”. In: *IEEE Sensors Journal* 20.18 (Sept. 2020). Conference Name: IEEE Sensors Journal, pp. 10345–10354. ISSN: 1558-1748. DOI: [10.1109/JSEN.2020.2993309](https://doi.org/10.1109/JSEN.2020.2993309).
- [20] Mirco Kolarczik et al. “Sideband pump-probe technique resolves nonlinear modulation response of PbS/CdS quantum dots on a silicon nitride waveguide”. In: *APL Photonics* 3.1 (Dec. 2017). Publisher: American Institute of Physics, p. 016101. DOI: [10.1063/1.5005490](https://doi.org/10.1063/1.5005490). URL: <https://aip.scitation.org/doi/full/10.1063/1.5005490> (visited on 07/27/2020).
- [21] Yan Liu et al. “Lock-in camera based heterodyne holography for ultrasound-modulated optical tomography inside dynamic scattering media”. In: *Applied Physics Letters* 108.23 (June 2016). Publisher: American Institute of Physics, p. 231106. ISSN: 0003-6951. DOI: [10.1063/1.4953630](https://doi.org/10.1063/1.4953630). URL: <https://aip.scitation.org/doi/abs/10.1063/1.4953630> (visited on 07/27/2020).

- [22] Andreas Mandelis. “Signal-to-noise ratio in lock-in amplifier synchronous detection: A generalized communications systems approach with applications to frequency, time, and hybrid (rate window) photothermal measurements”. In: *Review of Scientific Instruments* 65.11 (Nov. 1994). Publisher: American Institute of Physics, pp. 3309–3323. ISSN: 0034-6748. DOI: [10.1063/1.1144568](https://doi.org/10.1063/1.1144568). URL: <https://aip.scitation.org/doi/10.1063/1.1144568> (visited on 07/27/2020).
- [23] G. Marriott et al. “Optical lock-in detection imaging microscopy for contrast-enhanced imaging in living cells”. en. In: *Proceedings of the National Academy of Sciences* 105.46 (Nov. 2008), pp. 17789–17794. ISSN: 0027-8424, 1091-6490. DOI: [10.1073/pnas.0808882105](https://doi.org/10.1073/pnas.0808882105). URL: <http://www.pnas.org/cgi/doi/10.1073/pnas.0808882105> (visited on 08/30/2020).
- [24] Mohammad Rafiq Muqri, Eric John Wilson, and Javad Shakib. “A Taste of Python – Discrete and Fast Fourier Transforms”. In: ISSN: 2153-5965. June 2015, pp. 26.123.1–26.123.11. ISBN: 978-0-692-50180-1. URL: <https://peer.asee.org/a-taste-of-python-discrete-and-fast-fourier-transforms> (visited on 07/27/2020).
- [25] Rami A. AL-Na'mneh and W. David Pan. “Five-step FFT algorithm with reduced computational complexity”. In: *Inf. Process. Lett.* (2007). DOI: [10.1016/j.ipl.2006.10.009](https://doi.org/10.1016/j.ipl.2006.10.009).
- [26] K. Neelakantan, S. Dattagupta, and K. P. Rajappan. “Signal to noise enhancement of lock-in amplifiers”. en. In: *Review of Scientific Instruments* 51.2 (Feb. 1980), pp. 251–252. ISSN: 0034-6748, 1089-7623. DOI: [10.1063/1.1136167](https://doi.org/10.1063/1.1136167). URL: <https://aip.scitation.org/doi/10.1063/1.1136167> (visited on 07/28/2020).
- [27] Pierre-Alain Probst and Alain Jaquier. “Multiple-channel digital lock-in amplifier with PPM resolution”. In: *Review of Scientific Instruments* 65.3 (Mar. 1994). Publisher: American Institute of Physics, pp. 747–750. ISSN: 0034-6748. DOI: [10.1063/1.1145096](https://doi.org/10.1063/1.1145096). URL: <https://aip.scitation.org/doi/10.1063/1.1145096> (visited on 07/28/2020).
- [28] Sudhakar Sah and Vinay Vaidya. “A Review of Parallelization Tools and Introduction to Easypar”. In: *International Journal of Computer Applications* 56 (Oct. 2012), pp. 30–34. DOI: [10.5120/8944-3108](https://doi.org/10.5120/8944-3108).
- [29] John H. Scofield. “Frequency-domain description of a lock-in amplifier”. In: *American Journal of Physics* 62.2 (Feb. 1994). Publisher: American Association of Physics Teachers, pp. 129–133. ISSN: 0002-9505. DOI: [10.1119/1.17629](https://doi.org/10.1119/1.17629). URL: <https://aapt.scitation.org/doi/10.1119/1.17629> (visited on 07/28/2020).
- [30] Manreet Sohal and Rasmeet Kaur. “Automatic Parallelization: A Review”. en. In: 2016, p. 5.
- [31] Maximiliano Osvaldo Sonnailon and Fabian Jose Bonetto. “Lock-in amplifier error prediction and correction in frequency sweep measurements”. In: *Review of Scientific Instruments* 78.1 (Jan. 2007). Publisher: American Institute of Physics, p. 014701. ISSN: 0034-6748. DOI: [10.1063/1.2428269](https://doi.org/10.1063/1.2428269). URL: <https://aip.scitation.org/doi/10.1063/1.2428269> (visited on 07/28/2020).
- [32] G. A. Stimpson et al. “An open-source high-frequency lock-in amplifier”. In: *Review of Scientific Instruments* 90.9 (Sept. 2019). Publisher: American Institute of Physics, p. 094701. ISSN: 0034-6748. DOI: [10.1063/1.5083797](https://doi.org/10.1063/1.5083797). URL: <https://aip.scitation.org/doi/10.1063/1.5083797> (visited on 07/28/2020).

- [33] Tao Sun et al. "High speed multi-frequency impedance analysis of single particles in a microfluidic cytometer using maximum length sequences". en. In: *Lab on a Chip* 7.8 (2007), p. 1034. ISSN: 1473-0197, 1473-0189. DOI: [10.1039/b703546b](https://doi.org/10.1039/b703546b). URL: <http://xlink.rsc.org/?DOI=b703546b> (visited on 01/06/2021).
- [34] Masahiko Taniguchi, Hai Du, and Jonathan S. Lindsey. "PhotochemCAD 3: Diverse Modules for Photophysical Calculations with Multiple Spectral Databases". en. In: *Photochemistry and Photobiology* 94.2 (2018). _eprint: <https://onlinelibrary.wiley.com/doi/pdf/10.1111/php.12862>. pp. 277–289. ISSN: 1751-1097. DOI: [10.1111/php.12862](https://doi.org/10.1111/php.12862). URL: <https://onlinelibrary.wiley.com/doi/abs/10.1111/php.12862> (visited on 09/13/2020).
- [35] Masahiko Taniguchi and Jonathan S. Lindsey. "Database of Absorption and Fluorescence Spectra of >300 Common Compounds for use in PhotochemCAD". en. In: *Photochemistry and Photobiology* 94.2 (2018). _eprint: <https://onlinelibrary.wiley.com/doi/pdf/10.1111/php.12860>. pp. 290–327. ISSN: 1751-1097. DOI: [10.1111/php.12860](https://doi.org/10.1111/php.12860). URL: <https://onlinelibrary.wiley.com/doi/abs/10.1111/php.12860> (visited on 09/13/2020).
- [36] Paul A. Temple. "An introduction to phase-sensitive amplifiers: An inexpensive student instrument". In: *American Journal of Physics* 43.9 (Sept. 1975). Publisher: American Association of Physics Teachers, pp. 801–807. ISSN: 0002-9505. DOI: [10.1119/1.9690](https://doi.org/10.1119/1.9690). URL: <https://aapt.scitation.org/doi/10.1119/1.9690> (visited on 07/28/2020).
- [37] D. A. Van Baak and George Herold. "Response of a lock-in amplifier to noise". In: *American Journal of Physics* 82.8 (July 2014). Publisher: American Association of Physics Teachers, pp. 785–797. ISSN: 0002-9505. DOI: [10.1119/1.4873915](https://doi.org/10.1119/1.4873915). URL: <https://aapt.scitation.org/doi/10.1119/1.4873915> (visited on 07/28/2020).
- [38] Xiaoyi Wang. "Sensitive digital lock-in amplifier using a personal computer". In: *Review of Scientific Instruments* 61.7 (July 1990). Publisher: American Institute of Physics, pp. 1999–2001. ISSN: 0034-6748. DOI: [10.1063/1.1141413](https://doi.org/10.1063/1.1141413). URL: <https://aip.scitation.org/doi/10.1063/1.1141413> (visited on 07/28/2020).
- [39] Lexing Ying. "Sparse Fourier Transform via Butterfly Algorithm". In: *SIAM Journal on Scientific Computing* 31.3 (Feb. 2009), pp. 1678–1694. ISSN: 1064-8275. DOI: [10.1137/08071291X](https://doi.org/10.1137/08071291X). URL: <https://doi.org/10.1137/08071291X> (visited on 08/03/2020).

Affiliation:

Daniel S. Slaughter
 Chemical Sciences Division
 Lawrence Berkeley National Laboratory
 1 Cyclotron Rd, Berkeley CA 94720
 E-mail: DSSlaughter@lbl.gov